Article

Neuron

Neural Encoding of Odors during Active Sampling and in Turbulent Plumes

Highlights

- Odor plumes are encoded by dynamic responses in second- and third-order olfactory neurons
- Plume stimuli drive short-term plasticity, increasing spike timing precision
- Locusts target odor with frequent antennal sweeps, giving more but weaker responses
- This active sampling strategy provides more information about odor location

Authors

Stephen J. Huston, Mark Stopfer, Stijn Cassenaer, Zane N. Aldworth, Gilles Laurent

Correspondence

gilles.laurent@brain.mpg.de

In Brief

How do neurons encode natural intermittent odors? Huston et al. find that such stimuli are efficiently encoded by dynamic neural responses, and that locusts actively increase the stimulus intermittency through targeted sampling behavior that improves information about odor location.

Huston et al., 2015, Neuron *88*, 403–418
October 21, 2015
http://dx.doi.org/10.1016/j.neuron.2015.09.007

CellPress

Neuron
Article

Neural Encoding of Odors during Active Sampling and in Turbulent Plumes

Stephen J. Huston,[1,5] Mark Stopfer,[2,5] Stijn Cassenaer,[3] Zane N. Aldworth,[2] and Gilles Laurent[4,*]
[1]Howard Hughes Medical Institute, Janelia Research Campus, Ashburn, VA 20147, USA
[2]National Institutes of Health, NICHD, 35 Lincoln Drive, MSC 3715, Bethesda, MD 20892, USA
[3]Division of Biology and Biological Engineering, California Institute of Technology, Pasadena, CA 91125, USA
[4]Max Planck Institute for Brain Research, Max-von-Laue-Strasse 4, 60438 Frankfurt am Main, Germany
[5]Co-first author
*Correspondence: gilles.laurent@brain.mpg.de
http://dx.doi.org/10.1016/j.neuron.2015.09.007

SUMMARY

Sensory inputs are often fluctuating and intermittent, yet animals reliably utilize them to direct behavior. Here we ask how natural stimulus fluctuations influence the dynamic neural encoding of odors. Using the locust olfactory system, we isolated two main causes of odor intermittency: chaotic odor plumes and active sampling behaviors. Despite their irregularity, chaotic odor plumes still drove dynamic neural response features including the synchronization, temporal patterning, and short-term plasticity of spiking in projection neurons, enabling classifier-based stimulus identification and activating downstream decoders (Kenyon cells). Locusts can also impose odor intermittency through active sampling movements with their unrestrained antennae. Odors triggered immediate, spatially targeted antennal scanning that, paradoxically, weakened individual neural responses. However, these frequent but weaker responses were highly informative about stimulus location. Thus, not only are odor-elicited dynamic neural responses compatible with natural stimulus fluctuations and important for stimulus identification, but locusts actively increase intermittency, possibly to improve stimulus localization.

INTRODUCTION

An important feature of olfaction and other sensory modalities is that natural sensory stimuli can be distorted by both environmental and behavioral events. Air or water turbulence breaks up an odor plume into concentrated packets or filaments of odor separated by pockets of very low odor concentration (Figure 1A; Murlis et al., 1992, 2000). Similarly, an animal's own sampling behaviors, including sniffing in mammals (Kepecs et al., 2006, Mainland and Sobel, 2006; Khan et al., 2012) and olfactory appendage flicking in crustaceans and insects (Figure 1B; Koehl, 2006), also impose intermittency on the olfactory stimulus. Little is known about how neural circuits encode the resulting stimuli, or about the behaviors animals use to interact with them.

The neural encoding of odors has usually been studied in the laboratory with controlled, regular, and sustained odor pulses. In the locust, this approach has revealed several features of stimulus coding that facilitate essential olfactory computations underlying odor identification and discrimination (reviewed in Laurent, 2002). These features include time-evolving neural responses that can outlast a stimulus (Laurent and Davidowitz, 1994; Wehr and Laurent, 1996; Laurent et al., 1996) and synchronization among neurons (Laurent and Naraghi, 1994), which is necessary for fine odor discrimination (Stopfer et al., 1997). It remains unclear, however, whether the olfactory processing mechanisms revealed in the laboratory can function effectively in more natural settings. The chaotic temporal structure of natural odor stimuli occurs at a timescale similar to that of neural coding features believed to contain information about the odor, and might therefore interfere with such neural representations (Vickers et al., 2001; Brown et al., 2005, Broome et al., 2006; Aldworth and Stopfer, 2015). Furthermore, all previous experiments have been performed on locusts with restrained antennae. It is therefore not known whether antennal odor sampling movements might themselves influence or interfere with neural spatiotemporal coding features.

To evaluate the effects of stimulus variability caused by odor plume turbulence and active sampling, we developed two novel experimental paradigms with locusts to isolate and characterize the two causes of intermittency. With a fixed-antenna wind tunnel preparation, we could investigate neural coding features elicited by chaotic, natural odor plumes. With an active-sampling preparation, in which locusts were free to flick their antenna through a linear odor filament and walk freely on a substrate, we could combine behavioral analyses with electrophysiology to address the functional significance of self-induced stimulus intermittency for olfactory coding.

We found that spatiotemporally structured neural responses efficiently encode both types of intermittent natural olfactory stimuli, and that active sampling behaviors take advantage of this ability by increasing intermittency to gain more information about an odor's location.

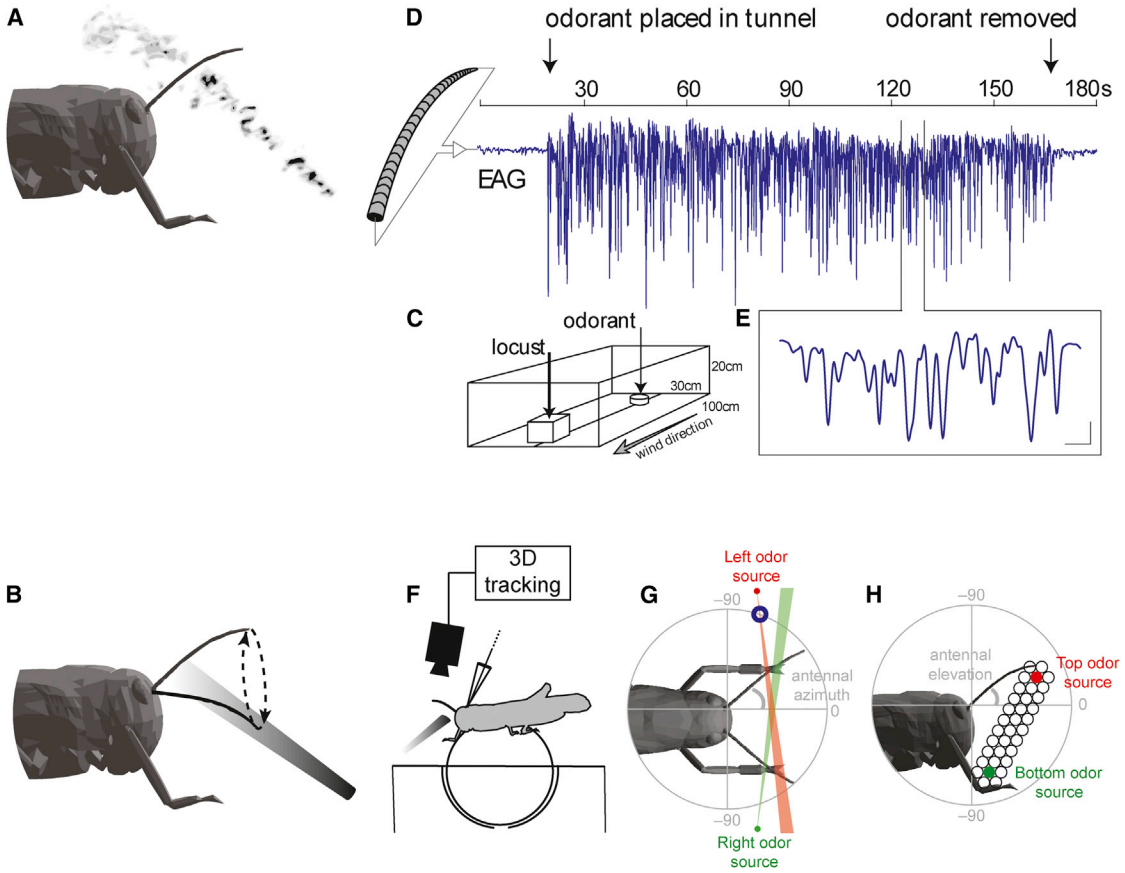

Figure 1. Studying Multiple Sources of Stimulus Intermittency

(A and B) Illustration of the two main sources of intermittency in natural olfactory stimuli: (A) turbulent odor plumes separate into intermittent filaments of high-concentration odor; (B) the animal's own sampling behavior, antennal flicking in the case of insects, results in intermittent stimulation even when exposed to a laminar odor plume.

(C) Diagram of the wind tunnel in which the locusts were exposed to turbulent odor plume stimuli.

(D) Example trace of an electroantennograms (EAG) recorded adjacent to the locust's intact antenna.

(E) Enlarged detail of the EAG shown in (D). Discrete EAG negative deflections indicate the transient presence of the odorant (scale bars, 300 ms; 0.05 mV; data low-pass filtered for display purposes).

(F) Experimental setup used for active sampling behavior and electrophysiology experiments. Tethered head-restrained locusts walked on a ball whose motion was tracked to measure walking speed and direction. Video records of the antennae were made from three different views, and the 3D antennal trajectory was reconstructed.

(G and H) Diagrams of the two stimulus configurations used during the active sampling experiments. Laminar odor plumes with known 3D positions were presented at different horizontal (G) and vertical (H) positions such that the locust was free to sweep its antenna in and out of the odorant while behavioral and electrophysiological measurements were made. Blue circle in (G) indicates the "odor edge": the closest point to the odor source that the antenna could reach along the odor plume.

RESULTS

Plumes Elicit Neural Oscillatory Synchronization and Temporal Patterning of PN Responses

We placed locusts with an immobilized antenna in a 1 m long wind tunnel and exposed them to turbulent odor plumes ~1 m downstream of the odor source (Figure 1C) while recording from second- and third-order olfactory neurons (PNs and mushroom body Kenyon cells, KCs, respectively) ipsilateral to the antenna. To monitor the arrival of windborne odor filaments near the animal's intact antenna, we recorded electroantennograms (EAGs) from the second, isolated antenna placed alongside the intact antenna (Vickers et al., 2001). This EAG signal tracked the local odor concentration imposed by the turbulent plume, allowing us to monitor the odor stimulus as it reached the locust (Figures 1A–1E). We examined whether the chaotic and intermittent pattern of odor filament exposure from a turbulent odor plume also resulted in temporal patterning, synchrony, and oscillations in antennal lobe and mushroom body neurons.

Exposing the locust to the turbulent odor plume led to series of brief bursts of odor stimulation, as assessed by negative deflections in the EAG (Figures 1D, 1E, and 2A). These bursts had a median duration of 159 ms, with a median interval of 157 ms (see

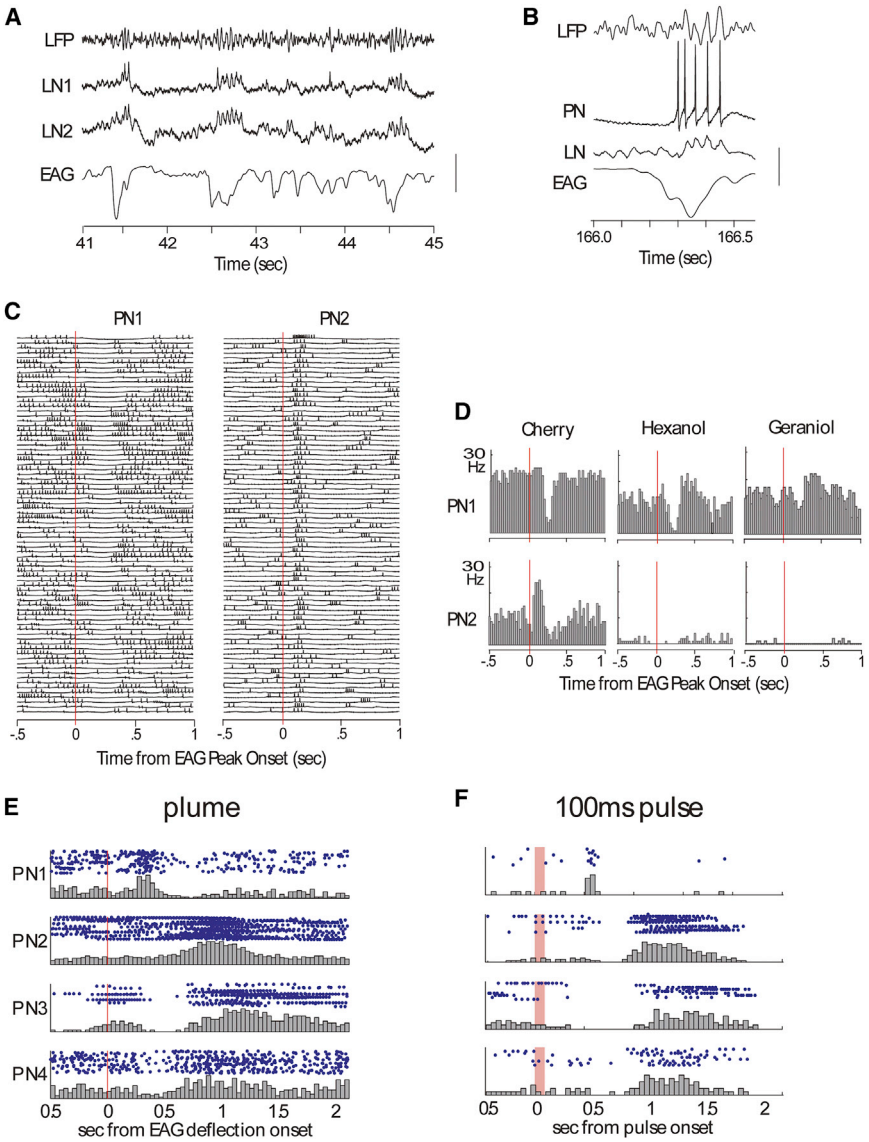

Figure 2. Plumes Elicit Oscillatory Synchrony and Temporal Patterning in Antennal Lobe Neurons

(A) Representative simultaneous recordings of LFP, EAG, and the intracellular activity of two LNs taken in the wind tunnel. LFP and LNs show several cycles of synchronous oscillation coincident with EAG deflections. Scale bar, LFP, 0.7; LN1 and LN2, 5; EAG, 0.2 mV.

(B) Simultaneous recordings of LFP, EAG and intracellular LN and PN activity. PN spikes coincide with EAG deflection and phase-lock to LN and LFP (PN-LFP coherence in Figure 3D). Scale bar, LFP, 0.4; PN, 22; LN, 6; EAG, 0.2mV.

(C and D) Slow temporal patterns in PNs. (C) One odorant (cherry) evoked different consistent patterns in two simultaneously-recorded PNs: 88 sweeps, aligned to EAG peak onsets. Note intensity of first response in PN2 (see also Figure 3). (D) Different odorants evoked different firing patterns in a given PN. Histograms constructed from the data in (C) reveal different response patterns for hexanol and geraniol (see text). Vertical line: time of EAG peak. Firing patterns outlasted corresponding EAG deflections.

(E and F) Odor plumes and controlled odor pulses elicited similar PN response patterns. Activity of four PNs recorded simultaneously during presentation of an odor plume (E), aligned as in Figure 2C) and then ten trials of brief, controlled puffs of the same odorant (F). Spikes times in blue, PSTHs in gray.

Figure S1 available online). The brief contacts with individual plume odor filaments, signaled by fast negative deflections of the EAG, led to bouts of oscillations in the mushroom body LFP, similar to those seen during longer controlled olfactory stimuli (e.g., Laurent and Naraghi, 1994), but briefer, typically lasting only three to six oscillation cycles (Figures 2A, 2B, and 3A). To quantify the relationship between LFP oscillatory power and odor filament encounters, we used a simple automated algorithm (see Experimental Procedures) that measured LFP power (14–34 Hz band) both during negative EAG deflections (indicative of odor filaments at the antenna) and during "flat" EAG segments (indicative of nonodorized air) (Figure 2A). These measurements showed that oscillatory power was significantly greater during EAG deflections (paired t test, $p < 0.001$, N = 200 trials, see Experimental Procedures), indicating that the plume's odor filaments were able to elicit bouts of oscillatory synchronization among the PNs and LNs of the antennal lobe.

We verified this synchronization directly with simultaneous intracellular recordings from LNs and PNs while the animal was exposed to odor plumes. During and immediately following individual EAG deflections, pairs of LNs showed subthreshold membrane potential oscillations were phase-locked to each other and to the LFP (33 LNs in 12 experiments; see examples in Figures 2A and 2B). During these deflections, some PNs were transiently inhibited, while others fired action potentials that were generally phase locked to the LNs and the LFP (example in Figure 2B). Odor elicited PN spikes (from ten PNs in ten experiments) were highly and significantly coherent with LFP oscillations (see below and Figure 3A).

Aligning PN responses to odor-filament contact revealed slow and multiphasic temporal patterns of spiking that outlasted the odor-filament contact (Figures 2C and 2D). These patterns of excitation and inhibition both depended on PN and odor identity and had profiles similar to those elicited by brief controlled pulses of the same odor (Figures 2E and 2F; Laurent and Davidowitz, 1994; Laurent et al., 1996). Thus, despite their intermittent nature, naturalistic turbulent odor plumes elicit the principal dynamic neural features identified using longer, controlled odor stimuli: oscillatory synchronization and slow temporal patterning of antennal lobe neurons.

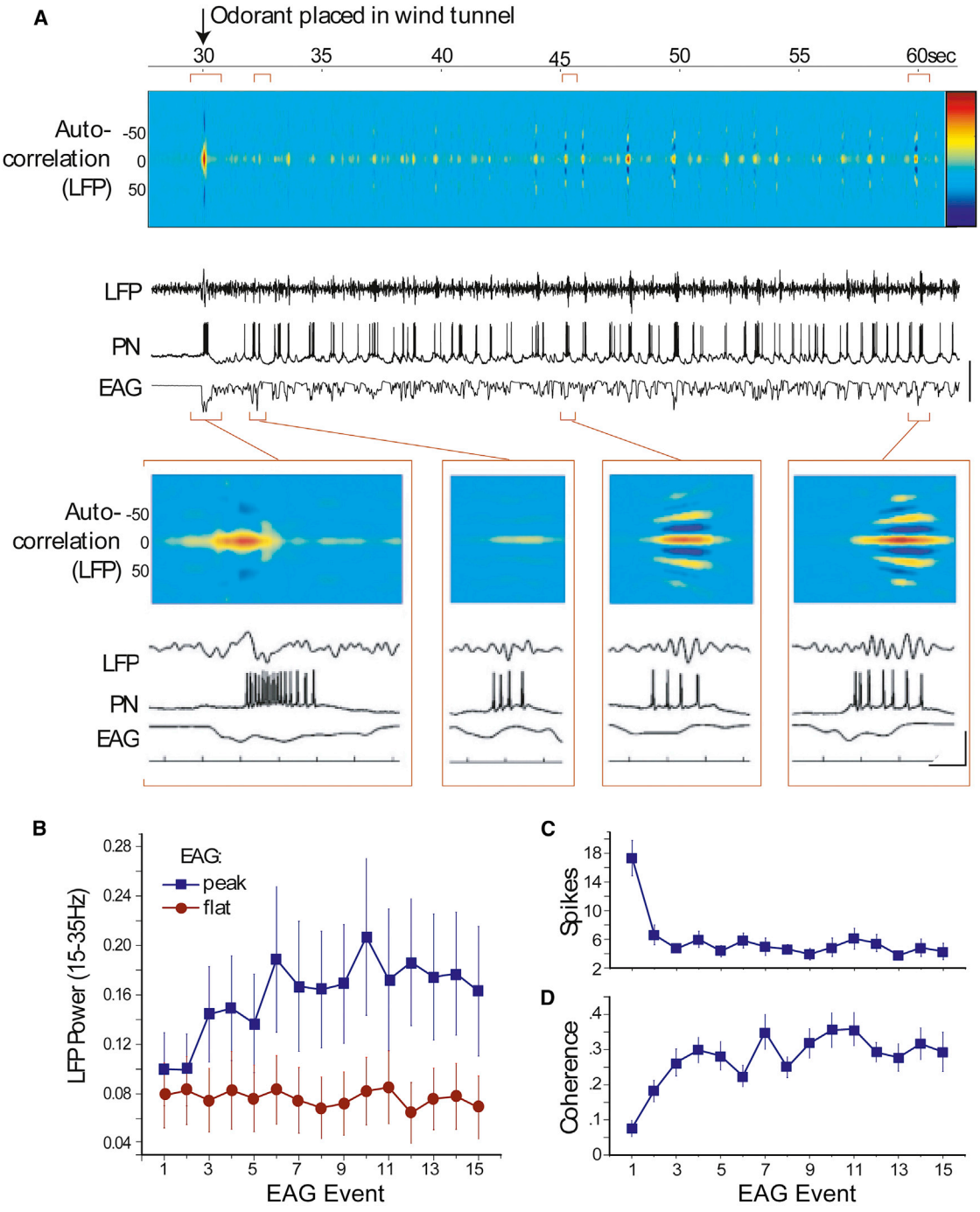

Figure 3. Olfactory Response Features Evolve during an Odor Plume

(A) Beginning of a wind-tunnel trial (odorant was placed into the wind tunnel at 30 s). Simultaneous LFP, EAG, and intracellular PN records, plotted with a color-coded sliding-window autocorrelation for the LFP. Recordings show LFP and PN responses coincident with EAG dips; autocorrelation shows gradual appearance of LFP oscillations (banding patterns with period ~50 ms = ~20 Hz). Autocorrelation color calibration, min = blue (−0.85); max = red (1.17). Scale bar (mV), LFP, 0.5; PN, 55; EAG, 0.15. Details in insets (red boxes). Note changes in LFP oscillatory power, decrease in PN response intensity, and increase in phase-locking between the PN and the LFP. Inset scale bar, horiz, 150 ms; vert, same as above.

(B) Increasing LFP oscillations: LFP power (15–35 Hz, $10^{-4}V^2$/Hz, means ± SEMs) during the first 15 EAG events averaged over all experiments (see Figure 2A). LFP power during "flat" EAG epochs (red circles) remained small, whereas power during "peak" EAG epochs (blue squares) gradually increased (n = 22 experiments; two-way ANOVA, F event type * event [14] = 1.94, $p < 0.02$).

(legend continued on next page)

Plumes Elicit Increasingly Sparse and Coherent Neural Responses to an Odor

During each 3 min plume exposure, the locust encountered multiple odor filaments resulting in successive EAG deflections. Previous work using controlled, long-duration odor stimuli showed that when the same odorant is repeatedly presented, each successive PN response contains fewer but better synchronized action potentials, correlated with stronger LFP oscillations and stronger phase-locking between PNs and LFP (Stopfer and Laurent, 1999). We tested whether the fluctuating and irregular structure of natural odor plumes led to a similar increase of PN spiking precision over the course of an odor plume presentation (Figure 3).

To measure the potential change in PN synchronization from one natural odor pulse to the next, we quantified LFP power in the 14–34 Hz band over the first 15 EAG deflections (odor filament contacts) and over the first 15 periods of "flat" EAG (no odor) (Figure 3B). The LFP power corresponding to flat EAG epochs remained small and constant (circles, Figure 3B), whereas LFP power measured during EAG deflections gradually increased, reaching asymptote after seven to ten deflections (squares, Figure 3B). The differences in LFP power were significant (n = 22 experiments; two-way ANOVA, F Event type * event (14) = 1.94, $p < 0.02$). Concomitant with this increase in LFP power, the intensity of each PN response (number of spikes/response) decreased, mainly after the first stimulus (Figure 3C). The change in spike number was significant (n = 10 experiments; one-way ANOVA, F (14,126) = 12.62, $p < 0.00001$). Furthermore, after the first few odor filament encounters, PN spikes phase locked more precisely with the LFP, evident in the increased coherence between PN firing and LFP oscillations (Figure 3D). This increase in coherence was significant (n = 10 experiments; one-way ANOVA, F (14,126) = 3.38; $p < 0.00001$) and reflects the growing oscillatory synchronization of many PNs. These changes and their time courses were similar to those evoked by repeated controlled odor pulses (Stopfer and Laurent, 1999). Taken together, these results indicate that the intermittency of natural, chaotic odor plumes result in "tuning" the antennal lobe circuits, leading to sparser but increasingly structured PN responses.

Readout of PN Responses by an Observer during Plume Stimulation

The above results reveal that the dynamic features of PN responses are efficiently driven by naturalistic odor plume stimuli. This suggests that, despite the intermittent nature of plume stimulation, it should be possible for downstream neurons to extract odor identity from the PN population response. We tested this first indirectly, by using classifiers to extract information about odor identity from the PN responses (Figure 4), and second directly, by using the downstream KCs as decoders of PN population output (Figure 5).

We first used a simple unsupervised classifier to determine whether the EAG-aligned PN firing patterns could be used to successfully identify the odorants within our stimulus set (Figure 4A; see Experimental Procedures). In Figure 4A, the lower group of traces shows the average classification performance of ten experiments, each of which incorporates the firing patterns from five simultaneously recorded PNs responding to odor plume stimulation; we found that classification performance greatly exceeded that predicted by chance alone (arrow, Figure 4A). Classification performance was even better in a single experiment combining the firing patterns of 13 simultaneously recorded PNs (Figure 4A, upper traces). We found that response patterns corresponding to larger EAG deflections (likely elicited by higher-concentration filaments) were more successfully classified than those aligned to weaker deflections. This finding is consistent with earlier work showing that, for a given odorant, higher concentrations elicit more separable responses (Stopfer et al., 2003). Although slightly longer samples permitted more successful classification, samples as brief as 150–200 ms (the median duration of EAG deflections) enabled classification success far above chance. These results demonstrate that plume-elicited PN firing patterns can in principle support odor recognition.

Because the above classifier used plume-evoked data sets for both training and classification, we next tested whether the encoding of odorant identity in regular *pulsed* stimuli could be used to decode odorant identity in *plumes*. We derived Gaussian mixed models (GMMs) of neuronal population responses (mean and covariance) from the responses of simultaneously recorded PNs to controlled *square pulses* of odorant with varying duration (0.1–2.0 s) and intensity (0.1%–100% concentration). The GMM was then used to "decode" the PN responses during *plume* stimulation by calculating the posterior probability (i.e., the probability of each model given observation of the corresponding PN responses) in a sliding window along the duration of a plume data epoch obtained in the wind tunnel. Alignment to odor filament hits was done with the EAG.

We found that these models, constructed from responses of groups of 5–19 PNs to regular pulses of an odor, accurately predicted the presence of that odor when given responses of the same PNs to odors presented as chaotic plumes in the wind tunnel (three experiments). In a representative experiment (Figures 4B–4D), after recording the responses of PNs to controlled odor pulses, we presented hexanol and then cherry odor to a locust in the wind tunnel. Figures 4B and 4C show that hexanol filaments, observed as downward deflections in the EAG, match the times when the PN response-based model, with very high levels of confidence, predicted the presence of hexanol rather than cherry. Figure 4D shows the average prediction for responses to both hexanol and cherry presentations, triggered by EAG deflections. The same log posterior probability ratio test was performed, with cross validation, entirely with PN

(C) Decreasing PN response intensity: number of spikes coincident with consecutive EAG dips decreased, mainly after the first encounter (means ± SEMs, n = 10 experiments; one-way ANOVA, F [14,126] = 12.62, $p < 0.00001$).

(D) Increasing PN-LFP phase-locking: coherence (see Experimental Procedures) between PN and LFP responses increased with consecutive EAG deflections (means ± SEMs, n = 10 experiments; one-way ANOVA, F [14,126] = 3.38; $p < 0.00001$).

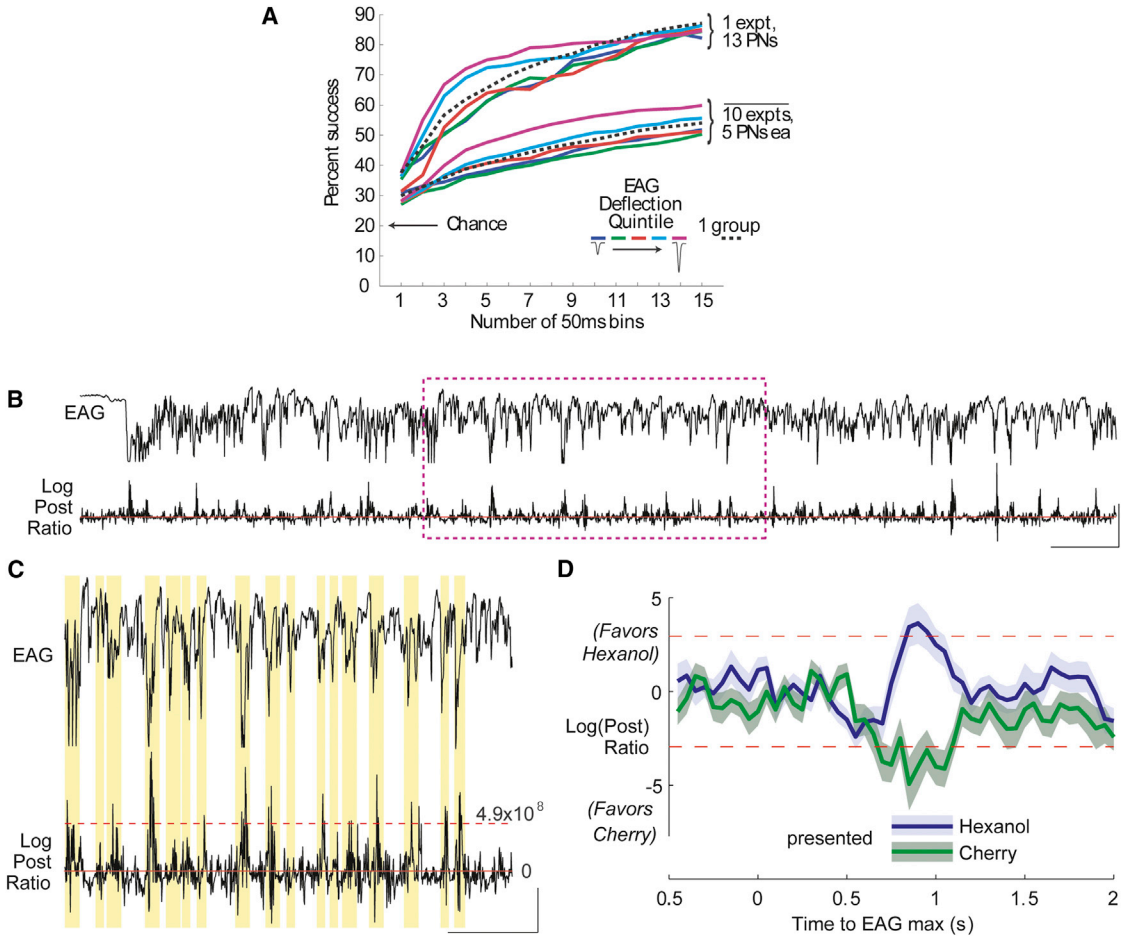

Figure 4. Decoding of PN Responses during an Odor Plume Using Unsupervised Classifiers

(A) An unsupervised algorithm could use plume-elicited PN responses to successfully classify odorants as one of five presented in the wind tunnel. Top set: classification success using 13 simultaneously recorded PNs. Colored lines: classification achieved using PN responses grouped by corresponding EAG amplitude (see legend); dotted line: classification using all responses, ungrouped. Bottom set: mean classification success for ten experiments, each containing five PNs each. Note that classification improved as more PNs, greater lengths of response (abscissa), and patterns corresponding to stronger EAG deflections were included in the analysis.

(B) A model constructed from responses of PNs to square pulses of odors could identify the odor present in a chaotic plume. Upper trace: EAG. Lower trace: instantaneous probability of identifying the odor in the plume based on the responses of the PNs. Solid red line: level at which models for either odor match the two odors equally well. Shown is the ratio of the natural logarithm of posterior probabilities from the two odorant models; positive deflections show when the model classifier selected the "correct" odorant, larger deflections indicate higher probability of matching the odorant (see Supplemental Experimental Procedures). Scale bars, vertical, 0.3 mV/80 log units; horiz., 10 s.

(C) Expanded view of boxed area in (B); the probability of selecting the correct odorant peaks when the odor filament crosses the antenna (shaded yellow). Solid red line: at this level, models for either odor match the two odors equally well; dashed red line: at this level, the model is 4.9×10^8 (e^{20}) times more likely to correctly match the presented odor. Scale bars, vertical, 0.15 mV/20 log units; horiz., 10 s.

(D) When filaments are present, the models accurately predict the odor. Average natural log of posterior probability ratio conditioned on negative EAG deflections of duration $\geq$200 ms. Blue and green lines: peaks in probability traces indicate times relative to EAG deflections at which the model assigns a high probability to the presence of a given odor. Shaded shaded areas: 95% confidence interval for model prediction. Red dashed lines: 95% probability for each odorant.

responses elicited by regular odor pulses, yielding qualitatively similar results (data not shown): when the EAG registered the presence of an odor pulse, the probability of correctly identifying the odor increased dramatically, with responses to high concentrations reaching log probability ratios as high as 40, matching the largest probabilities obtained with odor plumes (see Figure 4C). Together, these results show that the PN response vectors evoked by controlled and pulsed odors can be used to decode quasicontinuously and with negligible error rate, the responses of those same PN assemblies to chaotic plumes containing these odors, suggesting that odor identity is encoded the same manner given either pulse or plume stimulation.

Finally, because signals from closely consecutive filaments within a plume might interact and affect the ability of the olfactory system to use certain temporal features of odor representations, we examined the correlation between inter-filament interval and

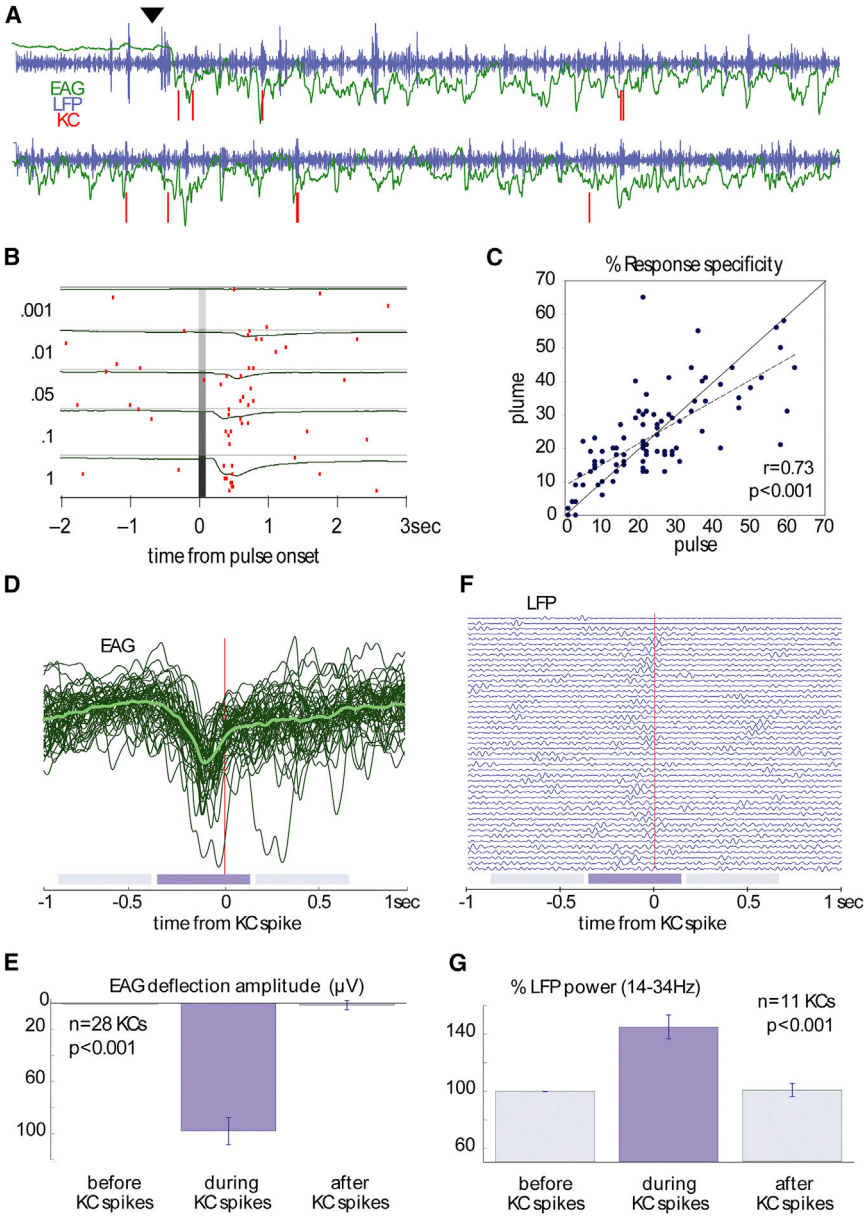

Figure 5. Decoding of PN Responses during an Odor Plume by Downstream KC Neurons

(A) Representative simultaneous recording shows KC spikes (red) correlated with strong EAG dips (presence of odor filament, green) and oscillatory bursts in the LFP (transient olfactory network synchrony, blue, band-pass 14-34 Hz). (A) shows two consecutive 30 s recordings. 7, odorant (cherry blend) placed in wind tunnel.

(B) KC in (A) also responded to brief (100 ms) pulses of odorant; in this KC, the highest concentration (see Experimental Procedures) elicited the most reliable responses. Fifteen trials of each concentration; green line: average EAG response; arbitrary scale is same for all five concentrations.

(C) KCs show similar response specificities when activated by brief pulses or by plumes. For all KC-odor pairs (blue dots, 28 KCs in ten experiments, four or five odors each), specificity (see Experimental Procedures) with pulse activation is plotted against specificity with plume activation. Pulse- and plume-elicited responses are highly correlated ($r = 0.73$, $p < 0.001$).

(D) Spikes in KC in (A) are correlated with EAG deflections. Green: EAG records (light green: mean) corresponding to all recorded KC spikes (red).

(E) Across all experiments, KC spikes tend to occur during EAG deflections (analyzed times indicated by horizontal shaded bars in D, difference from mean "before") (means ± SEMs, 28 KCs in ten experiments; two-way ANOVA: $F[2,569] = 90.2$, $p < 0.0001$).

(F) Spikes in KC in (B) are correlated with LFP oscillations. Blue traces: LFP records (band-pass 14–34 Hz) aligned with corresponding KC spikes (red line, t = 0).

(G) Across all experiments, KC spikes are correlated with LFP oscillations; percent of "before" mean oscillatory power ($10^{-4}V^2$/Hz) in 14–34 Hz band, integrated over times indicated by color bars in (D), was significantly greater during KC spikes than at other times (means ± SEMs, 11 KCs in six experiments, two-way ANOVA: $F[2,329] = 21.48$, $p < 0.0001$).

the ability to discriminate between odors. We examined the relationship between peak discrimination value—assessed by the ratio of posterior probabilities—in a small (1.5 s) window following deflections in the EAG trace, and interfilament intervals. This analysis revealed that consecutive filaments interact to a small but significant ($R^2 = 0.034$, $p = 0.0017$) extent. The slope of the regression line was 1.6 with a *y* intercept value of 17.3, indicating that for each additional 1 s between filament arrivals, the classifier was, on average, about 5.50 ($e^{1.6}$) times more likely to correctly identify the odorant. Thus, it becomes easier for the olfactory system to identify an odorant as consecutive filaments are spaced farther apart in time within a plume. Note however that, even when consecutive filaments completely overlapped, the classifier was 3.26*107 ($e^{17.3}$) times more likely to correctly identify the odorant than when no filament was present. Thus, the impact of interfilament interval is small relative to the olfactory system's overall discrimination ability.

Readout of PN Responses by Kenyon Cells during Plume Stimulation

KCs are targets and natural decoders of the PNs' output. Because KCs are highly selective for certain odors presented in controlled conditions (Perez-Orive et al., 2002; Shen et al., 2013) and because they each sample about 50% of the PN population (Jortner et al., 2007), their responses should reveal whether circuits can extract odor identity information from PN ensembles during odor plume stimulation. How, then, do KCs respond to odor plumes? In 32 wind-tunnel experiments, we

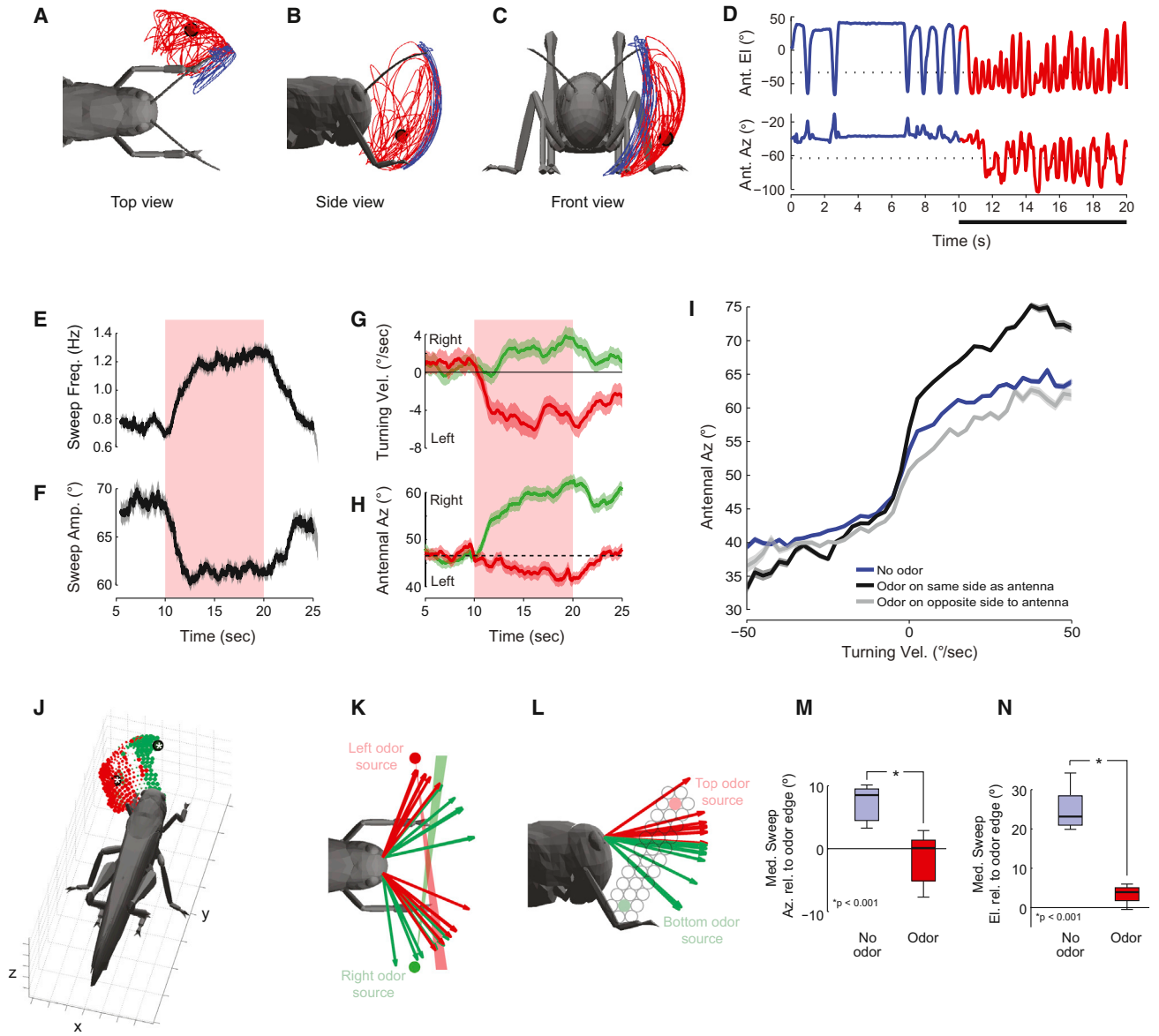

Figure 6. Locusts Actively Target Their Antennae to Odorant Locations

(A–C) Representative 3D antennal tip trajectory during 10 s presentation of clean air (blue) and odor (red). Black circles marked with white asterisks: the "odor edge" (nearest point to the odor source along the odor stream that the antennae could reach).

(D) The same antennal trajectory in coordinates of antennal azimuth and elevation. Dotted lines: odor edge position.

(E and F) Average antennal sweep frequency (E) and amplitude (F) over an odor presentation trial ($p < <0.001$ for both Wilcoxon signed rank tests that frequency or amplitude was the same before and during odor, n = 330 trials, 14 locusts). Orange shading: epoch when odor was on.

(G and H) Average walking turning velocity (G) and antennal azimuth position (H) of the locust during trials with odor presentation to either the right (green line) or left (red line) of the animal ($p < <0.001$ for both two-sided Wilcoxon rank sum tests that walking direction or antennal azimuth was same during odor delivery from the left and right, n = 214, six locusts). Orange shaded area: as in (E) and (F). In (G), positive turning velocity is to the locust's right, negative to the left. In (H), data are plotted with respect to the right antenna, and horizontal dotted line indicates average preodor antennal azimuth. In (E)–(I), data are shown as mean values (solid line) ± SEM (shaded).

(I) Odor-induced change in antennal position is not explained purely by walking direction. Turning velocity indicates whether the locust is turning toward (positive values) or away from (negative values) the odor. Average azimuth angles of the antennae are plotted for three different conditions: ipsilateral odor presentation (black), contralateral odor presentation (gray), and nonodor (blue) conditions. Note that some standard error bars are too small to be seen.

(J) Example of how changing odor location changes the locations sampled by the left antenna of an individual locust. Small spheres: the antennal tip positions that were more common during odor delivery from either the animal's left (red) or right (green). Sphere radii are proportional to the difference between the number of frames the antennal tip spent at a given location during the odor and nonodor conditions. Black circles marked with white asterisks: left and right odor edges.

(legend continued on next page)

recorded from 205 KCs, and found that KCs responded sparsely in the presence of odor plumes. Figure 5A shows a typical example of a KC responding to a plume of cherry odorant (green traces indicate EAG responses, blue traces indicate the LFP, and red tick marks indicate spikes of one KC). In 290 s of exposure to the odor plume (60 s shown), this KC fired only 49 times. To compare the odor specificity of KCs to plumes or long puffs, we delivered both types of stimuli in the same experiments. We found that KC spikes elicited by plume filaments predicted responses to pulse delivery, and vice versa. The KC shown in Figure 5A, for example, responded most reliably to puffs of the highest concentration of cherry odor (Figure 5B), though at times relative to pulse onset that varied with concentration (see also Stopfer et al., 2003; Gupta and Stopfer, 2014). To quantify this comparison, we made similar measures from 28 KCs in ten experiments. All KCs so tested showed comparable sensitivities to odorants (see Experimental Procedures) whether tested with brief pulses or odor plumes; sensitivities were significantly correlated with one another ($r = 0.73$; $p < 0.001$; Figure 5C).

Our simultaneous recordings further revealed that KC spikes usually occurred during EAG deflections. For example, Figure 5D shows EAG activity around every spike recorded from the KC in Figure 5A (red line, time of KC spikes; dark green, every corresponding EAG trace; light green, average EAG response). Note that, for this KC-odor pair, the delay between EAG deflection and KC spike was consistent. We observed the co-occurrence of EAG deflections and KC spikes in all of our paired recordings; these results are quantified in Figure 5E (28 KCs in ten experiments; two-way ANOVA, $F(2,569) = 90.2$, $p < 0.001$). We found that the delay between an EAG-triggered KC spike varied from KC to KC, and from odor to odor (see also Stopfer et al., 2003); our perispike sample window was sufficiently long (0.5 s) to account for this variation. Our results thus show that KC spikes are elicited by odor filament encounters. Finally, we found that KC spikes usually (but not always) occurred during transient increases in LFP oscillatory power. For example, Figure 5F shows LFP recordings around every spike recorded from the KC shown in Figure 5A. Again, all of our paired recordings revealed this co-occurrence: summary data from 11 KCs in six experiments show significantly increased LFP power (14–34 Hz) during KC spiking (Figure 5G; two-way ANOVA: $F(2,329) = 21.48$, $p < 0.0001$). Thus, KCs tend to spike during periods of odor-elicited transient PN synchrony of sufficient coherence to cause observable LFP oscillations.

In summary, KCs responded to odor plumes sparsely, during odor filament encounters, and when PNs were transiently synchronized. These observations are consistent with those previously obtained using controlled odor pulses (Laurent and Naraghi, 1994; Perez-Orive et al., 2002; Stopfer et al., 2003; Brown et al., 2005) and show that, despite the intermittency of natural odor plumes, important information such as odor identity is still reliably passed on from second- to third-order neurons of the olfactory system. In fact, the increase in spike timing precision invoked by repeated stimulation from sequential odor filaments in a chaotic plume may even serve to enhance coding precision of the third-order neurons (Bazhenov et al., 2005).

Locusts Actively Sample Odors

Odor stimuli are also discretized by an animal's own sampling behavior. For example, many insects repeatedly sweep their antennae through odor fields (Figure 1B). To study selectively the effects of these movements, we developed a method to measure a tethered locust's antennal and walking behavior in response to localized odor stimuli. We simultaneously measured walking direction and the 3D position of both antennae relative to the known 3D location of thin laminar odor or air streams (Figures 1F–1H and S2). This enabled us to calculate when a locust's freely moving antenna contacted the odor and, thus, to reconstruct the animal's self-imposed odor-stimulus time course. In the absence of odor, locusts often engaged in "clean-air" antenna sweeping. When an odor was presented, locusts increased their antennal sweep frequency (Figures 6A–6E), reduced their sweep amplitude (Figures 6D and 6F), walked (Figure 6G), and moved their antenna toward the odor source (Figures 6H and 6I).

In some insect species, antennal position covaries with walking direction (Dürr and Ebeling, 2005). To assess whether the antennal movements we observed were actively targeting odors rather than simply being correlated with turning movements, we examined antennal behavior as locusts made turns both in the presence and absence of an odor filament. For any given turning velocity toward the odor (positive turning velocities), we found that antennae swept closer to the odor source than they would sweep during the same turning velocity without odor (Figure 6I); this difference was dramatically reduced when turning away from the odor (negative turning velocities). In addition, we found the positioning of the antennae matched that of the odor source regardless of the source's location in both azimuth (Figures 6J and 6K) and elevation (Figure 6L). In the presence of an odor, antennae swept primarily through the point along the reachable odor filament closest to the odor source, a position we termed the "odor edge" (blue circle in Figure 1G). The angle between the position of each antennal sweep and the odor edge decreased in the presence of an odor in both azimuth (Figure 6M) and elevation (Figure 6N; two-sided Wilcoxon rank sum test that odor and non-odor data came from the same distribution, $p < 0.001$ for both azimuth and elevation). Thus, the locust's odor-induced changes in antennal movements reflected a targeted, active sampling strategy rather than a simple fixed change in antennal behavior.

(K) Arrows give the circular mean of the antennal tip distributions like that shown in J for six locusts (214 trials). Arrow color indicates whether odor delivery was from the left (red) or right (green). Mean position arrows are shown for both left and right antennae (as indicated by the position of the arrow base).

(L) Circular means of the antennal angles that were more common when odor was delivered from above (red) or below (green) the locust (data from eight locusts, 232 trials, two-sided Wilcoxon rank sum test that data from different odor positions came from the same distribution: $p < 0.001$ for both azimuth and elevation conditions).

(M and N) Distribution of per-trial median azimuth (M) and elevation (N) distances between the antenna during a sweep and the odor edge. Note that the antennal sweeps occur closer to the odor edge (y value = 0) in the odor condition (red) than the nonodor condition (blue).

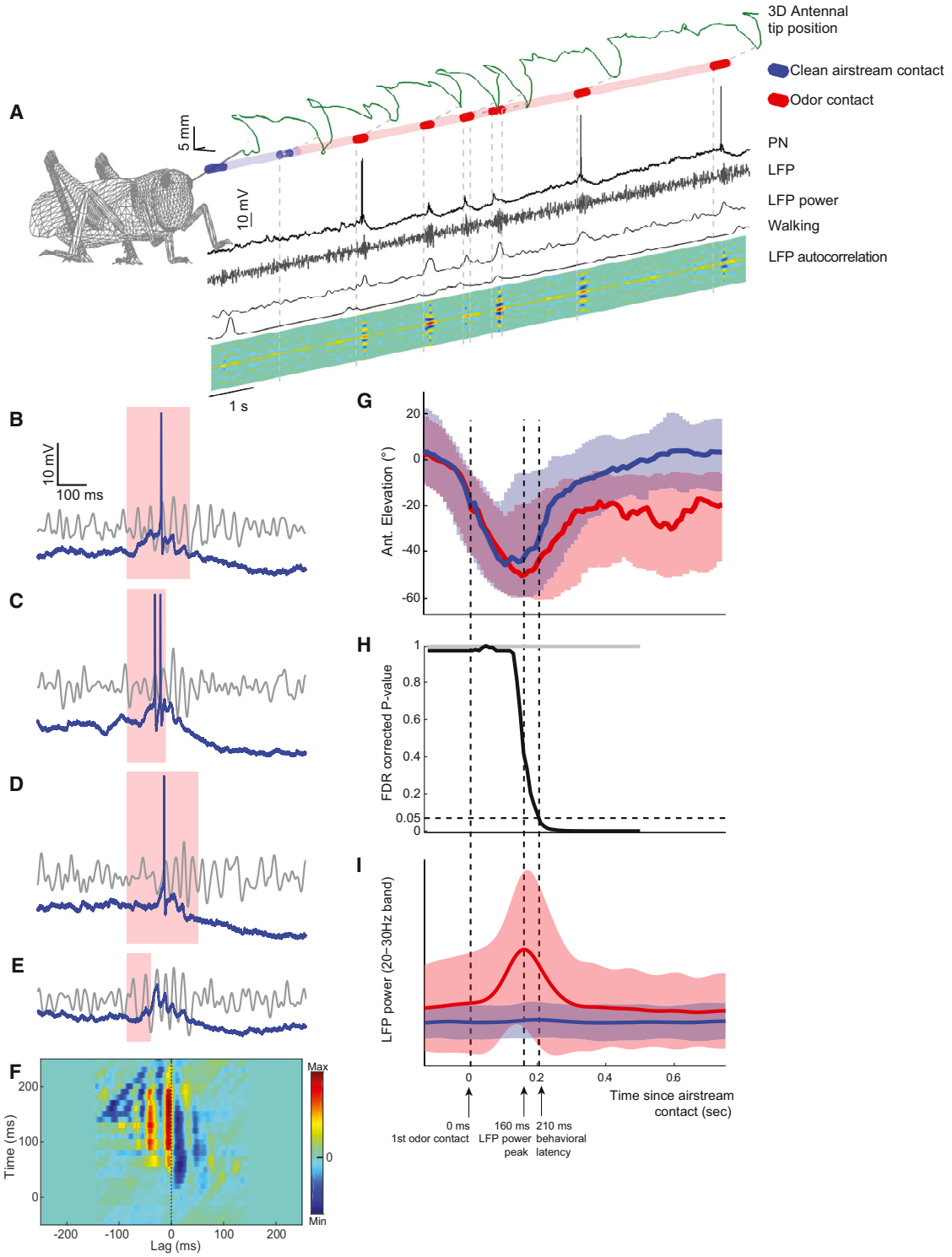

Figure 7. Simultaneous Electrophysiology and Behavior in Walking Animal

(A) Example projection neuron (PN) intracellular recording made as the locust actively sampled a laminar odor stream. Top green trace: 2D projection of the 3D antennal tip trajectory. Colored tube indicates airstream location (blue, clean air; red, odor turned on). Saturated segments indicate when antenna intersected the airstream. Vertical dotted lines: start of odor contact periods. Shown below (top to bottom) are the simultaneously recorded membrane potential of a PN, the LFP, LFP power (5–55 Hz band), forward component of walking, and LFP autocorrelation. Responses to antennal odor contact can be seen in both the PN and LFP traces.

(legend continued on next page)

Neural Responses during Active Sampling Behavior

To determine the effect of active sampling on the responses of central olfactory neurons to odor, we made intracellular recordings from individual PNs and recorded LFPs from the mushroom body as the locust moved its antenna freely in and out of a laminar odor stream (Figure 7A, as in the behavioral experiments described in Figure 6). From results shown in Figure 6, we knew that our odor stimuli were sufficient to induce detectable orienting responses. We investigated whether the locust's own sampling of such a stimulus was sufficient to induce the dynamic neural response features observed in our natural-plume experiments (Figures 2A and 2B). As with odor-plume stimuli (Figure 3A), when the antenna contacted the odor stream, transient oscillatory waves appeared in the LFP that briefly outlasted the odor contact (Figures 7A–7E); PN action potentials and subthreshold membrane potential oscillations were phase-locked to the LFP during these events (Figures 7B–7F). Thus, we could identify stimuli that elicit behavior, record neural responses to these stimuli, and observe when the locust's freely moving antenna first contacted the odor stream. For the first time in locusts, we could now compare behavioral and neural latencies directly.

For each period when the air stream was odorized, we noted when the antenna first contacted the odor stream (t = 0 in Figures 7G–7I). After this initial contact, the antenna's trajectory started to diverge from its normal clean-air sweeping trajectory (red versus blue, Figure 7G). To estimate the latency of the locust's behavioral response to the odor, we measured the probability that the antennal positions at each time point following initial odor contact came from the equivalent distribution of positions during a clean-air sweep. Defining behavioral latency as the time between initial odor contact and the time when this probability fell below p = 0.05 (Figures 7G and 7H; see Supplemental Experimental Procedures), we found this behavioral latency to be 210 ms (Figures 7G and 7H; N = 6 locusts, n = 125 trials). When data from individual locusts were treated separately, this latency fell within 140–510 ms. Thus, locusts changed their antennal sweeping behavior after a single sweep through an odor. We found that LFP power in the 10–30 Hz band peaked on average 160 ms after each odor contact (Figure 7I). Thus, the behavioral change occurred ~50 ms, or one LFP oscillation cycle, after the peak in neural response, measured as LFP power. Previous work has shown that this time encompasses the transient period when responses of PNs evolve rapidly and the PN population activity is most informative about odor identity (Mazor and Laurent, 2005).

Reconstructing Odor Filament Location from Neural Response during Active Sampling

Locusts displayed a range of antennal-sweep motions when sampling odors (Figure 6). Using simultaneous measures of antennal movements and neural activity, we sought to identify the specific movements that led to the strongest neural responses to odors. Sorting antennal sweeps by their corresponding LFP responses revealed that the greatest LFP power occurred during shallow antennal sweeps through the odor stream (Figure 8A)—that is, during sweeps that resulted in longer odor contacts (Figure 8B). This suggests the locust could, in principle, increase the signal-to-noise ratio of the odor-elicited neural response by adjusting its antennal sweeps to obtain longer odor samples. Our behavioral measures showed that locusts do *not* do this; in fact, the median per-sweep contact duration actually decreased by 16% in the presence of odor (Figure 8C). Instead, locusts increased sweep frequency in the presence of odor (Figure 6E), resulting in an increase in odor-contact frequency: the median contact frequency increased by 49% in the presence of an odor (Figure 8D).

We investigated possible consequences of this increase in antennal sweep frequency and odor targeting by the antenna (Figure 6). Our behavioral experiments suggested that locusts use information about odor location to guide walking direction and antennal search behavior. To test whether neural responses contain information about odor location, we compared simultaneous measures of neural activity and antennal position. We found that graphing antennal position color coded by 10–30 Hz LFP power (corrected for the 160 ms neural delay) revealed a reasonable estimate of the true odor location (Figure 8E). To further quantify the information about odor location provided by the neural responses to a given antennal sweep sequence, we calculated the normalized mutual information (NMI; Studholme et al., 1999; Pluim et al., 2003; see Supplemental Experimental Procedures) between the LFP-power-based reconstruction (Figure 8E) and the actual known odor location (inset, Figure 8E). NMI scores range from 0 to 1, from neural activity providing no information to perfect information about odor position at all locations across the spherical surface surrounding the locust. (NMI never reaches 1 because the locust's antennae cannot reach all locations around its head.)

Thus we compared different sweep sequences across trials to determine the patterns providing most neural information about odor location. When a locust encounters an odor, it both increases its antennal sweep frequency and shifts its sweep

(B–E) High-resolution segment of traces in (A), showing LFP (gray) and PN (blue) responses during odor contact periods (orange). Note that both PN action potentials (B–D) and PN subthreshold responses (E) are phase-locked to the odor-induced LFP oscillation cycles.

(F) Odor-triggered average crosscorrelation between PN membrane potential and LFP.

(G–I) Combined behavioral and neural data from different experiments to estimate their relative latencies from odor contact. (G) Median (dark lines) antennal elevation during the antenna downsweep that resulted in the first contact with either odor (red) or the clean airstream (blue) in each trial (125 trials, six locusts). Shaded regions: interquartile range of the antennal elevation. (H) Odor and nonodor average antennal trajectories diverge after the initial airstream/odor contact (t = 0, first vertical dashed line). The time of this divergence is quantified by plotting the false discovery rate (FDR) corrected probability that the odor and nonodor elevation data at each time point come from the same distribution. We defined the behavioral latency as the time when this probability drops below p = 0.05 (horizontal dashed line). As a control we performed the same analysis on adjacent sweeps that both occurred during the no-odor condition (light gray line). (I) Mean standardized LFP power in the 10–30 Hz band occurring after odor (red) or clean airstream (blue) contact (data from eight locusts, 189 trials, error bars are standard deviations, y axis has arbitrary units). The LFP power peaks on average at 160 ms, i.e., 50 ms before the first statistically distinguishable change in behavior (210 ms).

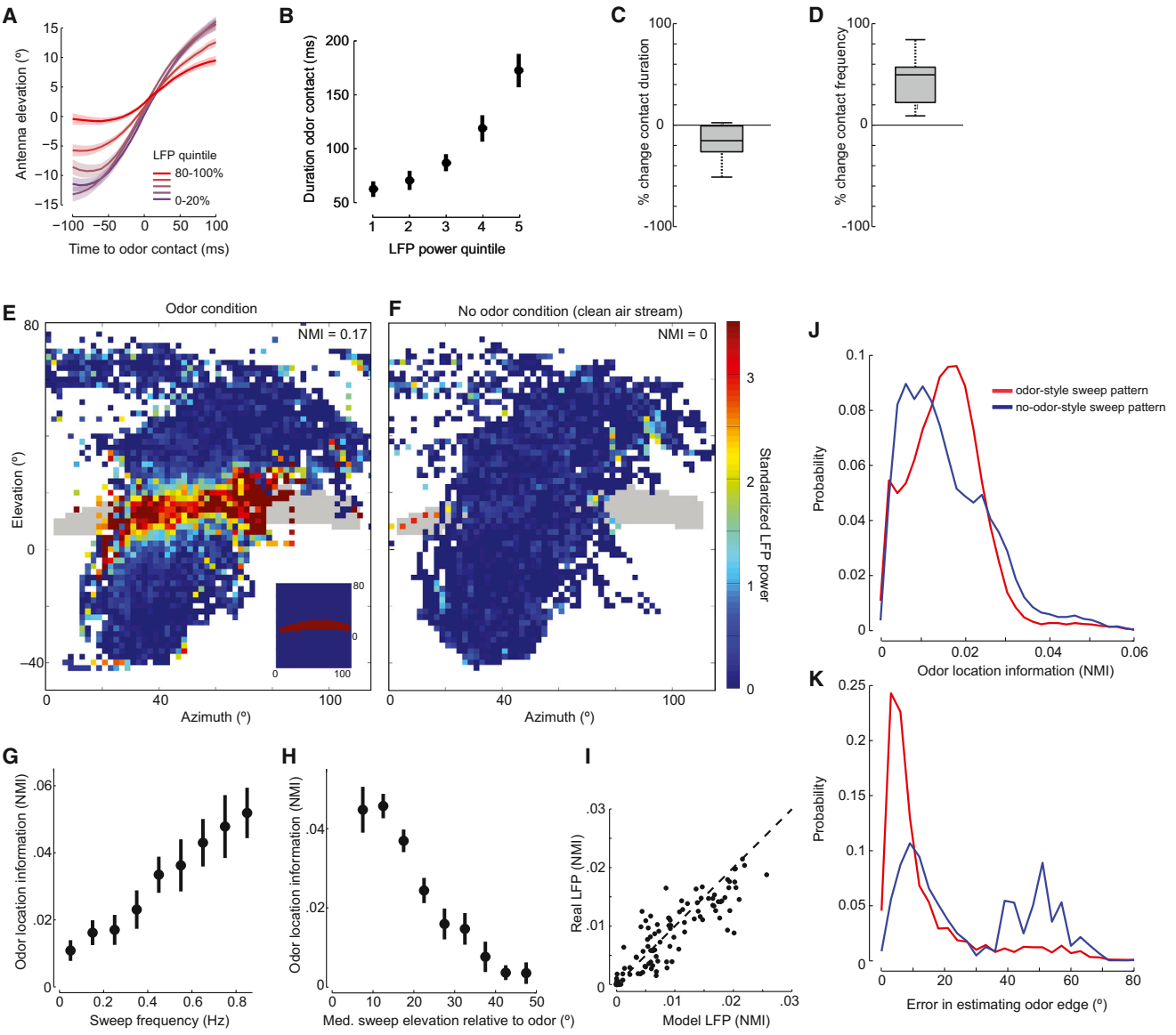

Figure 8. Neural Consequences of Active Sampling

(A and B) Stronger neural responses are driven by shallower antennal sweeps with a longer duration of odor contact. (A) Antennal tip elevations during each upsweep through the odor are binned by strength of the resulting LFP power and the mean (±SEM) sweep trajectory plotted for each quintile of LFP power (downsweeps showed a similar result, data not shown). A flatter line indicates a shallower sweep through the odor. Data from eight locusts, 189 10 s trials, 1,228 odor contacts. (B) The mean (±SEM) duration of odor contact per sweep is plotted for each of the LFP quintiles in (A) (overall median odor contact duration = 63 ms, data from both up- and downsweeps).

(C and D) Odor-induced changes in antennal sweep patterns result in shorter, higher-frequency odor contacts. Data are the percent change between odor and no-odor conditions for median per-sweep airstream contact duration (C), and median contact frequency (D) (six locusts, 107 trials.)

(E and F) Odor filament location can be reconstructed from LFP power and antennal movements. Colored points show the antennal tip positions visited over an entire experiment (53 10 s trials, bin size = 2° × 2°). Points are color coded by the standardized 10–30 Hz LFP power that resulted from visiting that location (LFP power is time shifted by 160 ms to correct for neural latency). (E) plots data from the odor condition; (F) plots data from when only the clean air stream was present. Background gray pixels indicate the location of the odor stream that the antenna was able to contact, shown in full in the inset of (E). The normalized mutual information (NMI, a measure of how much information the LFP reconstruction contains about the odor location) was 0.17 and 0 for the odor and no-odor conditions, respectively.

(G) The per-trial NMIs computed as in (E) and plotted against the per-trial average antennal sweep frequency. An increase in sweep frequency correlates with an increase in information about the odor location.

(H) Per-trial NMI as a function of median elevation distance between the antenna and the odor during all sweeps in a trial. Changes in the elevation angle of antennal sweeps to bring it closer to the odor, as was seen in the behavioral experiments, correlate with an increase in information about the odor location. Data from eight locusts, 189 10 s trials, 1,228 odor contacts; error bars, SEM.

(legend continued on next page)

elevation to a point closer to the odor (Figure 6). Both of these changes strongly correlate with an increase in information about odor location as measured by NMI (Figures 8G and 8H). This observation led us to hypothesize that odor-induced changes in antennal behavior increase the amount of information about odor location available in the neural response. To test this hypothesis, we used a simple model of odor-elicited LFPs to estimate what the LFP response would have been, had an odor been present during the antennal movements generated in the no-odor trials. This model computed the kernel that best predicted real LFP power responses given the odor stimulus time course and noise matched to the data (see Supplemental Experimental Procedures). We validated the model by showing that NMI values based on real LFP data correlated well with those produced by the model given the same antennal movements (Figure 8I; Pearson's correlation coefficient, r = 0.88). We applied this model to antennal movements measured in both the "odor" and the "no-odor" conditions as if odor were present in both. Compared to the "no-odor" condition, using the antennal movements from the "odor" condition yielded a probability distribution with NMI values shifting higher (Figure 8J), even when trials were truncated so that both odor and no-odor conditions contained the same number of sweeps (Figure S3). This indicates that, indeed, neural information about odor location was enhanced by the odor-induced change in antennal movements.

Finally, by finding the maximum local contrast in the LFP reconstruction image, we estimated the location of the edge of the odor stream closest to the odor source (see Supplemental Experimental Procedures). Our behavioral experiments had suggested that the "odor edge" (Figure 1G) was an important stimulus feature, potentially providing information about the walking direction required to approach the odor source (Figure 6). We found that the antennal movements during odor presentations resulted in reduced error in estimates of the odor edge location (Figures 8K and S3). Thus, results from both experiments and modeling suggest that the antennal sweep patterns locusts use in the presence of an odor provide more information about both the overall location of the odor and the location of its edge, a specific, behaviorally relevant stimulus feature.

DISCUSSION

Most animals, including humans, encounter natural odors as a series of complex, intermittent patterns of stimuli. Such intermittency is generated both externally by turbulent air or water and internally by active sampling behaviors such as sniffing in mammals (Kepecs et al., 2006; Mainland and Sobel, 2006), antennule flicking in crustaceans (Koehl et al., 2001; Koehl, 2006), wing fanning in moths (Loudon and Koehl, 2000), or head-casting in insect larvae (Gomez-Marin et al., 2011). Like the external world, these sampling behaviors have the consistent consequence of providing the animal's olfactory system with repeated, intermittent, discrete odor samples (Kay and Laurent, 1999; Spors and Grinvald, 2002; Cang and Isaacson, 2003; Rinberg et al., 2006a; Verhagen et al., 2007; Carey et al., 2009; Carey and Wachowiak, 2011; Shusterman et al., 2011; Khan et al., 2012; Nagel et al., 2015).

Despite this stimulus intermittency, many species can rapidly identify (e.g., Uchida and Mainen, 2003; Abraham et al., 2004; Rinberg et al., 2006b; Bhandawat et al., 2010) and locate (e.g., Budick and Dickinson, 2006; Porter et al., 2007; Willis, 2010; Gaudry et al., 2013) odorants. Thus, a fundamental question is how the nervous system processes odor stimuli with such complex structures. This question becomes especially interesting because many species use complex neural dynamics to encode odor information. How do the neural dynamics interact with those of a stimulus, and how is an animal's sampling behavior adapted to these neural codes? Using two new experimental paradigms in a well-studied insect, we separated the two sources of natural odor intermittency and studied their respective effects on neural processing.

Natural Intermittent Stimuli Reliably Drive Temporal Features of Olfactory Coding

Because of the technical challenges they present, naturalistic plume stimuli have rarely been used to study olfactory coding (Khan et al., 2012). In vertebrate experiments, odor presentations are often sustained, but rendered intermittent by a superimposed breathing or ventilation rhythm (e.g., Rinberg et al., 2006a; Shusterman et al., 2011). Studies based on intermittent but well-controlled odor stimuli have been fruitful in insects (Stopfer and Laurent, 1999; Vickers et al., 2001; Brown et al., 2005; Martelli et al., 2013; Riffell et al., 2014) where many features of dynamic neural encoding have been characterized (Laurent, 2002). Here, we used the locust olfactory system, in which antennal odor receptors are more readily accessible to the external world than are the internal, turbinate-bound receptors of vertebrates, to examine how naturalistic odor plumes, like those encountered in natural settings such as forests and fields (Murlis et al., 2000), are encoded and decoded by second- and third-order olfactory neurons. It has been suggested (Vickers et al., 2001) that the complex temporal structures of natural odor stimuli would

(I) A simple model to predict the LFP power responses and thus the NMI from the measured antennal movements and known odor location. The NMI values generated by the model are strongly correlated with the NMI values obtained from the real LFP power measured during the same antennal movements (data from 53 trials, one locust).

(J) Odor-location reconstruction quality differs between antennal movements displayed in odor and no-odor behavioral conditions. We used the model described in (I) to estimate the NMI values that would result from the antennal sweep movements recorded in the behavioral dataset if odor had been present during both odor and no-odor conditions. The red line gives the probability of each NMI value when using the sweep patterns seen during odor presentation; the blue line results from using the sweep patterns seen during the no-odor condition. The curve peak shifts to better odor-location reconstructions (higher NMI) when antennal sweep patterns observed during the odor condition are used. Data are from six locusts; trials where the antenna did not contact the odor are excluded.

(K) Using the same model LFP power data as in (J), we computed, for each trial, an estimate of the location of the odor edge (closest point to the odor source that was reachable by the antenna). The angular distance between this estimate and the actual odor edge was calculated. Probability of obtaining different values of angle error plotted for the odor (red) and no-odor (blue) sweep patterns. On average, antennal movements that occurred during the odor condition, rather than those during the no-odor condition, resulted in a better estimate of the odor edge location.

interfere with dynamical features of olfactory neuronal responses, such as the slow temporal patterns of spiking and periodic synchronization that had been revealed mainly by regular and sustained odor stimuli (reviewed in Laurent, 2002), casting doubt on the functional relevance of neural response timing.

Our results establish that chaotic odor plumes drive olfactory circuitry to generate all the spatiotemporal features of PN and KC responses characterized earlier under sustained, stationary stimulation regimes (Laurent and Davidowitz, 1994; Stopfer and Laurent, 1999; Wehr and Laurent, 1996; Laurent et al., 1996; Stopfer et al., 1997, 2003; Perez-Orive et al., 2002; Mazor and Laurent, 2005). Despite introducing variance into odor-encoding temporal response patterns, the very brief, irregular odor encounters generated by chaotic plume stimulation provide a highly efficient input for generating odor-specific, distributed, spatiotemporal patterns of synchronous activity in antennal lobe neurons that outlasted the transient odor filament encounters. These brief population firing patterns efficiently drove their downstream decoder neurons the KCs in an odor-specific manner and could be used successfully for unsupervised odor classification. Over the duration of an odor plume, the temporal precision of the PN responses significantly increased, with successive filament encounters eliciting fewer but more precisely aligned spikes in PNs, and stronger ~20 Hz oscillations in the LFP. Our results indicate that odor identification is robust to natural stimulus intermittency and suggest that the same spatiotemporal activity patterns that have been observed with sustained odor exposure are likely to be part of the locust's processing of natural olfactory stimuli.

An Active and Adaptive Odor-Sampling Strategy

In addition to the natural stimulus intermittency of odor plumes, many species impose intermittency through olfactory sampling behavior. Insects have been shown to adjust the movements of their antennae when an odor is presented (e.g., Nishiyama et al., 2007), and such movements have been suggested to reflect active odor sampling (e.g., Wilson, 2008; Wachowiak, 2011). It was not known, however, whether these movements represent targeted olfactory sampling or rather, nonspecific manifestations of a change in the animal's state, triggered by the stimulus.

We established a new preparation to enable recording from olfactory neurons while the animal actively scanned its surroundings with its odor-sensitive antenna. Our results show that the locust's antennal flicking does represent a directed odor sampling strategy. We found that antennal movement trajectories shifted significantly as the antenna completed its first sweep through an odorized air stream. The timing of this response was similar to the latency for "one-sniff" behaviors observed in rodents (Johnson et al., 2003; Uchida and Mainen, 2003; Wesson et al., 2008). The brief behavioral latency we observed, with odor-triggered antennal movements redirecting within 50 ms after the peak of LFP power and within 200 ms of odor contact, indicates that the behavioral shift began during the initial "transient phase" of the PN population's response. At this time neural responses undergo rapid odor-specific changes and provide, from an ideal decoder's point of view, the most information about odor identity (Mazor and Laurent, 2005). Similarly, locusts sweep their antennae at the same ~0.8 Hz frequency (Figure 6E) at which PN responses are most informative about the dynamics of a stimulus (Geffen et al., 2009). Thus, the animal's odor-elicited sampling behaviors are aligned with the optimal informational window in the PN ensemble. We did not find any evidence for anticipatory or modulated PN activity during active sampling.

An inherent tradeoff exists between the quantity and the quality of sensory samples that can be taken within a given time: increasing sampling frequency produces more samples, but if all the samples are shorter, they will each produce noisier estimates. Indeed, we found that fast and steep antennal sweeps evoked weaker neural responses than slow and shallow sweeps that allowed longer contact with the odor. Why, then, do locusts increase the frequency rather than the duration of antennal odor sampling, when this reduces the strength of the neural odor responses, effectively trading sample quality for quantity? First, weak population responses can be informative, provided that they are temporally precise (Stopfer et al., 1997; Stopfer and Laurent, 1999; Perez-Orive et al., 2002). Second, we found that this rapid sampling behavior enabled a better reconstruction of the stimulus location from the resulting neural responses by providing weak samples at many locations as opposed to strong samples at a few locations. Thus, our results show that the increased stimulus intermittency introduced by antennal active sampling behaviors actually serves to enhance encoding of stimulus location, information that is essential to the survival of the animal. Additionally, because odor plumes change rapidly, serial sampling strategies enable the efficient exploration of an unstable olfactory space. It would be interesting to determine whether active sampling behaviors in other sensory modalities such as saccadic eye movements or whisking in rodents make similar tradeoffs between quality and number of sensory samples to improve stimulus localization.

Taken together, our results suggest that the formats of neural representations of odors and antennal sampling behaviors are well matched to provide both identification and localization of natural odor stimuli. Not only does the locust olfactory system efficiently encode naturalistic intermittent odor stimuli with information-bearing dynamic neural responses, but locusts exploit this ability by actively adjusting their sampling behavior to increase the intermittency of stimulation, thus providing the animal with more information about stimulus location. The relevance of such changes in sampling frequency after odor detection (e.g., Wesson et al., 2009) is strongly indicated by recent results with rats tracking odor trails (Khan et al., 2012). Additional sampling and decoding strategies, such as bilateral comparisons, have also been shown to be relevant both in rodents (Khan et al., 2012) and in flies (Gaudry et al., 2013). The fascinating similarity between strategies, if not mechanisms, employed by such distant animal species should eventually help us converge on the underlying fundamental principles of olfactory coding.

EXPERIMENTAL PROCEDURES

Full details are provided in the Supplemental Information.

Animals

Results were obtained from 83 adult locusts (*Schistocerca americana*) of both sexes and prepared as described in Laurent and Davidowitz (1994) and Stopfer et al. (2003).

Electrophysiology

EAGs were recorded using chlorided silver-wire electrodes placed in an isolated antenna wired to a DC amplifier (Brownlee). Intracellular recordings were made using sharp glass electrodes. KCs, some PNs and some LFPs were recorded using tetrodes or silicone probes. Data were analyzed offline.

Odor Stimulation and Conditions

Odors were presented to immobilized animals in a 1 m long wind tunnel or with a conventional olfactometer, or in animal walking on an air-supported trackball via a set of directed and parallel tubing forming laminar flow in front of its freely moving antennae. Odors were fresh flowers, freshly cut wheatgrass or liquid odorants ("green" odorants (Visser et al., 1979): 1-hexanol, 1-heptanol, cis-3-hexen-1-ol, trans-2-hexen-1-ol, hexanal, 2-heptanone, 1-octanol, and geraniol (Sigma); 3-pentanone (Aldrich); and mint and cherry (LorAnn Oils).

Video Acquisition

Movies were recorded at 100 fps and 468 × 490 resolution (Basler a602f camera). Image acquisition was controlled through Matlab. Illumination was provided by an array of red LEDs (Thor Labs). Two mirrors placed on either side of the locust at ~45° provided three different views in all, allowing antennal position reconstruction in 3D. Camera frames were synchronized with the trackball and electrophysiology data with a TTL pulse.

Data Analysis

Methods are given in full in the Supplemental Information.

SUPPLEMENTAL INFORMATION

Supplemental Information includes three figures, one movie, and Supplemental Experimental Procedures and can be found with this article at http://dx.doi.org/10.1016/j.neuron.2015.09.007.

AUTHOR CONTRIBUTIONS

M.S., S.J.H., S.C., and G.L. conceived the experiments and wrote the manuscript. M.S. performed the odor plume experiments, and M.S. and Z.N.A. analyzed them. S.J.H. performed the active sampling behavior experiments. S.J.H. and S.C. performed the active sampling electrophysiology experiments, and S.J.H. analyzed the resulting data. G.L. managed and supervised the work.

ACKNOWLEDGMENTS

This work was supported by the NIH and the Max Planck Society (G.L.), by grants from the U.S. Office of Naval Research (G.L. and S.C.), and by an intramural NIH-NICHD grant (M.S.). We thank Kristin Branson for advice on the automated antennal tracking and the Laurent Lab and Simon Laughlin for discussion and comments.

Received: December 3, 2014
Revised: May 11, 2015
Accepted: August 31, 2015
Published: October 8, 2015

REFERENCES

Abraham, N.M., Spors, H., Carleton, A., Margrie, T.W., Kuner, T., and Schaefer, A.T. (2004). Maintaining accuracy at the expense of speed: stimulus similarity defines odor discrimination time in mice. Neuron *44*, 865–876, http://dx.doi.org/10.1016/j.neuron.2004.11.017.

Aldworth, Z.N., and Stopfer, M.A. (2015). Trade-off between information format and capacity in the olfactory system. J. Neurosci. *35*, 1521–1529, http://dx.doi.org/10.1523/JNEUROSCI.3562-14.2015.

Bazhenov, M., Stopfer, M., Sejnowski, T.J., and Laurent, G. (2005). Fast odor learning improves reliability of odor responses in the locust antennal lobe. Neuron *46*, 483–492, http://dx.doi.org/10.1016/j.neuron.2005.03.022.

Bhandawat, V., Maimon, G., Dickinson, M.H., and Wilson, R.I. (2010). Olfactory modulation of flight in Drosophila is sensitive, selective and rapid. J. Exp. Biol. *213*, 3625–3635, http://dx.doi.org/10.1242/jeb.053546.

Broome, B.M., Jayaraman, V., and Laurent, G. (2006). Encoding and decoding of overlapping odor sequences. Neuron *51*, 467–482, http://dx.doi.org/10.1016/j.neuron.2006.07.018.

Brown, S.L., Joseph, J., and Stopfer, M. (2005). Encoding a temporally structured stimulus with a temporally structured neural representation. Nat. Neurosci. *8*, 1568–1576, http://dx.doi.org/10.1038/nn1559.

Budick, S.A., and Dickinson, M.H. (2006). Free-flight responses of Drosophila melanogaster to attractive odors. J. Exp. Biol. *209*, 3001–3017, http://dx.doi.org/10.1242/jeb.02305.

Cang, J., and Isaacson, J.S. (2003). In vivo whole-cell recording of odor-evoked synaptic transmission in the rat olfactory bulb. J. Neurosci. *23*, 4108–4116.

Carey, R.M., and Wachowiak, M. (2011). Effect of sniffing on the temporal structure of mitral/tufted cell output from the olfactory bulb. J. Neurosci. *31*, 10615–10626, http://dx.doi.org/10.1523/JNEUROSCI.1805-11.2011.

Carey, R.M., Verhagen, J.V., Wesson, D.W., Pírez, N., and Wachowiak, M. (2009). Temporal structure of receptor neuron input to the olfactory bulb imaged in behaving rats. J. Neurophysiol. *101*, 1073–1088, http://dx.doi.org/10.1152/jn.90902.2008.

Dürr, V., and Ebeling, W. (2005). The behavioural transition from straight to curve walking: kinetics of leg movement parameters and the initiation of turning. J. Exp. Biol. *208*, 2237–2252, http://dx.doi.org/10.1242/jeb.01637.

Gaudry, Q., Hong, E.J., Kain, J., de Bivort, B.L., and Wilson, R.I. (2013). Asymmetric neurotransmitter release enables rapid odour lateralization in *Drosophila*. Nature *493*, 424–428, http://dx.doi.org/10.1038/nature11747.

Geffen, M.N., Broome, B.M., Laurent, G., and Meister, M. (2009). Neural encoding of rapidly fluctuating odors. Neuron *61*, 570–586, http://dx.doi.org/10.1016/j.neuron.2009.01.021.

Gomez-Marin, A., Stephens, G.J., and Louis, M. (2011). Active sampling and decision making in Drosophila chemotaxis. Nat. Commun. *2*, 441, http://dx.doi.org/10.1038/ncomms1455.

Gupta, N., and Stopfer, M. (2014). A temporal channel for information in sparse sensory coding. Curr. Biol. *24*, 2247–2256.

Johnson, B.N., Mainland, J.D., and Sobel, N. (2003). Rapid olfactory processing implicates subcortical control of an olfactomotor system. J. Neurophysiol. *90*, 1084–1094, http://dx.doi.org/10.1152/jn.00115.2003.

Jortner, R.A., Farivar, S.S., and Laurent, G. (2007). A simple connectivity scheme for sparse coding in an olfactory system. J. Neurosci. *27*, 1659–1669, http://dx.doi.org/10.1523/JNEUROSCI.4171-06.2007.

Kay, L.M., and Laurent, G. (1999). Odor- and context-dependent modulation of mitral cell activity in behaving rats. Nat. Neurosci. *2*, 1003–1009, http://dx.doi.org/10.1038/14801.

Kepecs, A., Uchida, N., and Mainen, Z.F. (2006). The sniff as a unit of olfactory processing. Chem. Senses *31*, 167–179, http://dx.doi.org/10.1093/chemse/bjj016.

Khan, A.G., Sarangi, M., and Bhalla, U.S. (2012). Rats track odour trails accurately using a multi-layered strategy with near-optimal sampling. Nat. Commun. *3*, 703–713, http://dx.doi.org/10.1038/ncomms1712.

Koehl, M.A., Koseff, J.R., Crimaldi, J.P., McCay, M.G., Cooper, T., Wiley, M.B., and Moore, P.A. (2001). Lobster sniffing: antennule design and hydrodynamic filtering of information in an odor plume. Science *294*, 1948–1951.

Koehl, M.A. (2006). The fluid mechanics of arthropod sniffing in turbulent odor plumes. Chem. Senses *31*, 93–105, http://dx.doi.org/10.1093/chemse/bjj009.

Laurent, G. (2002). Olfactory network dynamics and the coding of multidimensional signals. Nat. Rev. Neurosci. *3*, 884–895, http://dx.doi.org/10.1038/nrn964.

Laurent, G., and Davidowitz, H. (1994). Encoding of olfactory information with oscillating neural assemblies. Science *265*, 1872–1875.

Laurent, G., and Naraghi, M. (1994). Odorant-induced oscillations in the mushroom bodies of the locust. J. Neurosci. *14*, 2993–3004.

Laurent, G., Wehr, M., and Davidowitz, H. (1996). Temporal representations of odors in an olfactory network. J. Neurosci. *16*, 3837–3847.

Loudon, C., and Koehl, M.A. (2000). Sniffing by a silkworm moth: wing fanning enhances air penetration through and pheromone interception by antennae. J. Exp. Biol. *203*, 2977–2990.

Mainland, J., and Sobel, N. (2006). The sniff is part of the olfactory percept. Chem. Senses *31*, 181–196, http://dx.doi.org/10.1093/chemse/bjj012.

Martelli, C., Carlson, J.R., and Emonet, T. (2013). Intensity invariant dynamics and odor-specific latencies in olfactory receptor neuron response. J. Neurosci. *33*, 6285–6297.

Mazor, O., and Laurent, G. (2005). Transient dynamics versus fixed points in odor representations by locust antennal lobe projection neurons. Neuron *48*, 661–673.

Murlis, J., Elkinton, J.S., and Cardé, R.T. (1992). Odor plumes and how insects use them. Annu. Rev. Entomol. *37*, 505–532.

Murlis, J., Willis, M.A., and Carde, R. (2000). Spatial and temporal structures of pheromone plumes in Fields and forests. Physiol. Entomol. *25*, 211–222.

Nagel, K.I., Hong, E.J., and Wilson, R.I. (2015). Synaptic and circuit mechanisms promoting broadband transmission of olfactory stimulus dynamics. Nat. Neurosci. *18*, 56–65.

Nishiyama, K., Okada, J., and Toh, Y. (2007). Antennal and locomotor responses to attractive and aversive odors in the searching cockroach. J. Comp. Physiol. A Neuroethol. Sens. Neural Behav. Physiol. *193*, 963–971, http://dx.doi.org/10.1007/s00359-007-0249-3.

Perez-Orive, J., Mazor, O., Turner, G.C., Cassenaer, S., Wilson, R.I., and Laurent, G. (2002). Oscillations and sparsening of odor representations in the mushroom body. Science *297*, 359–365.

Pluim, J.P.W., Maintz, J.B.A., and Viergever, M.A. (2003). Mutual-information-based registration of medical images: a survey. IEEE Transac. Med. Imaging *22*, http://dx.doi.org/10.1109/TMI.2003.815867.

Porter, J., Craven, B., Khan, R.M., Chang, S.-J., Kang, I., Judkewitz, B., Volpe, J., Settles, G., and Sobel, N. (2007). Mechanisms of scent-tracking in humans. Nat. Neurosci. *10*, 27–29, http://dx.doi.org/10.1038/nn1819.

Riffell, J.A., Shlizerman, E., Sanders, E., Abrell, L., Medina, B., Hinterwirth, A.J., and Kutz, J.N. (2014). Sensory biology. Flower discrimination by pollinators in a dynamic chemical environment. Science *344*, 1515–1518, http://dx.doi.org/10.1126/science.1251041.

Rinberg, D., Koulakov, A., and Gelperin, A. (2006a). Sparse odor coding in awake behaving mice. J. Neurosci. *26*, 8857–8865, http://dx.doi.org/10.1523/JNEUROSCI.0884-06.2006.

Rinberg, D., Koulakov, A., and Gelperin, A. (2006b). Speed-accuracy tradeoff in olfaction. Neuron *51*, 351–358, http://dx.doi.org/10.1016/j.neuron.2006.07.013.

Shen, K., Tootoonian, S., and Laurent, G. (2013). Encoding of mixtures in a simple olfactory system. Neuron *80*, 1246–1262.

Shusterman, R., Smear, M.C., Koulakov, A.A., and Rinberg, D. (2011). Precise olfactory responses tile the sniff cycle. Nat. Neurosci. *14*, 1039–1044, http://dx.doi.org/10.1038/nn.2877.

Spors, H., and Grinvald, A. (2002). Spatio-temporal dynamics of odor representations in the mammalian olfactory bulb. Neuron *34*, 301–315, http://dx.doi.org/10.1016/S0896-6273(02)00644-X.

Stopfer, M., and Laurent, G. (1999). Short-term memory in olfactory network dynamics. Nature *402*, 664–668, http://dx.doi.org/10.1038/45244.

Stopfer, M., Bhagavan, S., Smith, B.H., and Laurent, G. (1997). Impaired odour discrimination on desynchronization of odour-encoding neural assemblies. Nature *390*, 70–74, http://dx.doi.org/10.1038/36335.

Stopfer, M., Jayaraman, V., and Laurent, G. (2003). Intensity versus identity coding in an olfactory system. Neuron *39*, 991–1004.

Studholme, C., Hill, D.L.G., and Hawkes, D.J. (1999). An overlap invariant entropy measure of 3D medical image alignment. Pattern Recognit. http://dx.doi.org/10.1016/S0031-3203(98)00091-0.

Uchida, N., and Mainen, Z.F. (2003). Speed and accuracy of olfactory discrimination in the rat. Nat. Neurosci. *6*, 1224–1229, http://dx.doi.org/10.1038/nn1142.

Verhagen, J.V., Wesson, D.W., Netoff, T.I., White, J.A., and Wachowiak, M. (2007). Sniffing controls an adaptive filter of sensory input to the olfactory bulb. Nat. Neurosci. *10*, 631–639, http://dx.doi.org/10.1038/nn1892.

Vickers, N.J., Christensen, T.A., Baker, T.C., and Hildebrand, J.G. (2001). Odour-plume dynamics influence the brain's olfactory code. Nature *410*, 466–470, http://dx.doi.org/10.1038/35068559.

Visser, J.H., Van Straten, S., and Maarse, H. (1979). Isolation and identification of volatiles in the foliage of potato, Solanum tuberosum, a host plant of the colorado beetle, Leptinotarsa decemlineata. J. Chem. Ecol. *5*, 13–25.

Wachowiak, M. (2011). All in a sniff: olfaction as a model for active sensing. Neuron *71*, 962–973, http://dx.doi.org/10.1016/j.neuron.2011.08.030.

Wehr, M., and Laurent, G. (1996). Odour encoding by temporal sequences of firing in oscillating neural assemblies. Nature *384*, 162–166, http://dx.doi.org/10.1038/384162a0.

Wesson, D.W., Carey, R.M., Verhagen, J.V., and Wachowiak, M. (2008). Rapid encoding and perception of novel odors in the rat. PLoS Biol. *6*, e82, http://dx.doi.org/10.1371/journal.pbio.0060082.

Wesson, D.W., Verhagen, J.V., and Wachowiak, M. (2009). Why sniff fast? The relationship between sniff frequency, odor discrimination, and receptor neuron activation in the rat. J. Neurophysiol. *101*, 1089–1102.

Willis, M.A. (2010). Odor plumes and animal orientation. In The Senses: A Comprehensive Reference, *Volume 4*, pp. 771–781, http://dx.doi.org/10.1016/B978-012370880-9.00127-4.

Wilson, R.I. (2008). Neural and behavioral mechanisms of olfactory perception. Curr. Opin. Neurobiol. http://dx.doi.org/10.1016/j.conb.2008.08.015.